Carbohydrate Polymers 171 (2017) 68–76

Contents lists available at ScienceDirect

Carbohydrate Polymers

journal homepage: www.elsevier.com/locate/carbpol

Hydrazine treatment improves conductivity of bacterial cellulose/graphene nanocomposites obtained by a novel processing method

Robert Ccorahua[a], Omar P. Troncoso[a], Sol Rodriguez[a], Daniel Lopez[b], Fernando G. Torres[a,*]

[a] Department of Mechanical Engineering, Pontificia Universidad Catolica del Peru, Lima 32, Peru
[b] Institute of Polymer Science and Technology, Spanish Council for Scientific Research (CSIC), Madrid, Spain

ARTICLE INFO

Article history:
Received 20 January 2017
Received in revised form 6 April 2017
Accepted 1 May 2017
Available online 2 May 2017

Keywords:
Bacterial cellulose
Reduced graphene oxide
Hydrazine
Electric conductivity

ABSTRACT

A novel method to prepare BC nanocomposites reinforced with reduced graphene oxide (RGO) is reported. A simple hydrazine treatment is shown to in-situ reduce the graphene oxide (GO) incorporated to BC films while increasing their conductivity. Raman spectroscopy was used to confirm the presence of graphene and assess the effect of the hydrazine treatment on its structure. XRD tests revealed no changes on BC structure. We hypothesize that this treatment removes the hydroxyl and epoxy groups present on the reduced graphene and increases the content of nonoxygenated carbon. These changes account for the increase in conductivity of the BC-based films, which behaved as an insulating material before the hydrazine treatment and reach an average conductivity value of 12 S/m after such a treatment.

1. Introduction

Electrically conductive polymers exhibit a range of properties that influence their value to high performance engineering. Their use in devices such as solar cells, fashioned from dyes and capacitors, may exhibit varying degrees of manipulability, toxicity and recyclability. Recently, researchers have shown an increased interest in using carbon based materials such as carbon nanotube and graphene in the development of electrically conducting composites. Graphene has been used to provide biopolymers such as starch, cellulose, bacterial cellulose, cotton, and carrageenan with good electrical conductivity (Bella, Mobarak, Jumaah, & Ahmad, 2015; Buraidah et al., 2010; Gan, Shang, Yuen, & Jiang, 2015; Lee, Han, Lee, & Jeong, 2016; Rudhziah, Ahmad, Ahmad, & Mohamed, 2015; Shi, Li, Chen, Han, & Yang, 2014; Tian et al., 2014; Zhang, Liu, Zheng, & Zhu, 2012) among others.

According to Zimmermann, Bordeanu, and Strub (2010), cellulose is the most abundant natural polymer, with a quantity of 1011 tons per year. Due to its availability and renewability, cellulose has been used to prepare graphene-reinforced composites with improved conductivity (Tian et al., 2014; Zhang et al., 2012). However, natural cellulosic fibers are composed of only 55–65% cellulose and further isolation and purification process are needed. By contrast, the bacteria from the *Gloconacetobacter* family produce a protective mat made from pure cellulose nanofibers.

Bacterial Cellulose (BC) has the same chemical structure as cellulose. Compared with plant-based cellulosic fibers, BC has an ultrafine nanosized three-dimensional fibrous network structure. BC fibrils are 10–100 nm in diameter. They have high crystallinity (~90%), and a highly hydrophilic characteristic due to the many hydroxyl groups on the surface (Gelin et al., 2007). In addition, the mechanical properties of BC nanofibers are higher than those of conventional natural cellulosic fibers (Lay et al., 2017).

Grande, Torres, Gomez, Troncoso et al. (2009) have reported the mechanical properties of bacterial cellulose (BC) films. They have found a mean traction resistance value of 241.42 ± 21.86 MPa, a maximum elongation of $8.21 \pm 3.01\%$ and a Young's modulus of 6.86 ± 0.32 GPa. Potential applications envisaged for BC include its use as reinforcing phase in membranes, acoustic diaphragms, strong paper, and biomaterials for biomedical applications (Hu, Chen, Yang, Liu, & Wang, 2011; Mormino & Bungay, 2003; Svensson et al., 2005; Yamanaka et al., 1989).

BC nanocomposites have also been used for the preparation of electrically conducting polymeric films. Feng, Zhang, Shen, Yoshino, and Feng, (2012) obtained BC/GO composites by blending sonicated suspensions of BC and GO with a conductivity of 1.1×10^{-4} S/m.

* Corresponding author.
E-mail address: fgtorres@pucp.pe (F.G. Torres).

http://dx.doi.org/10.1016/j.carbpol.2017.05.005
0144-8617/

Nandgaonkar et al. (2014), Si et al. (2014), Luo et al. (2014) and Zhu, Li, He, and Duan (2015) prepared BC/RGO. They used an agitated culture medium that allows the fibers to be synthetized while being combined with RGO. Liu et al. (2015) ultrasonicated BC and GO in anhydrous N, N'-dimethyl formamide. After vigorous stirring with dicyclohexylcarbodiimide they obtained covalent cross-linked networks of BC/GO with a conductivity of 171 S/m.

Several processing routes have been reported for the preparation of BC nanocomposites. Some processing routes include the disintegration of the BC gel in order to blend it as a standard nanofiller (Iguchi, Yamanaka, & Budhiono, 2000; Yano, 2005). Feng et al. (2012) disintegrated a rehydrated BC gel using an ultrasonication technique. They blended the BC suspension with a GO suspension to prepare BC/GO. However, the disintegration of the native BC nanofibers can alter the properties of BC films as the coherent 3D network is destroyed and the aspect ratio (length/diameter) of individual cellulose nanofibers is reduced.

A different processing route investigated in our laboratory consists of introducing a second phase to the BC culture medium during the development of the BC nanofibers (Grande, Torres, Gomez, & Carmen Bañó, 2009). Using this processing route, starch, hydroxyapatite, collagen and poly-ly-sine have been successfully incorporated into BC networks that would be prime candidates for biomedical applications (Culebras et al., 2015; Grande, Torres, Gomez, Carmen Bañó, 2009; Grande, Torres, Gomez, Troncoso et al., 2009). In this paper, we report a novel processing route in which the natural BC structure, instead of being disintegrated, is dried in the presence of graphene oxide (GO) platelets to incorporate them into the films.

This paper aims to report a novel processing route that takes advantage of the natural network structure of BC to incorporate graphene oxide (GO) platelets into a pristine cellulose network. As far as the authors are concerned, there is no previous report on a methodology for the preparation of electrically conductive BC/GO composites that avoids the disintegration of the native BC network. In order to provide these BC/GO composites with electrical conductivity, a simple hydrazine treatment to in-situ reduce the incorporated graphene oxide sheets was developed. The resultant BC nanocomposite films which incorporate reduced graphene oxide (RGO) platelets were characterized by Fourier transform infrared spectroscopy (FTIR), X-ray diffraction (XRD), Raman spectroscopy, scanning electron microscopy (SEM), thermogravimetric analysis (TGA), differential scanning calorimetry (DSC), electrical conductivity tests and mechanical measurements. The effect of various hydrazine treatment times and the content of GO and RGO on the properties of the BC nanocomposites was investigated.

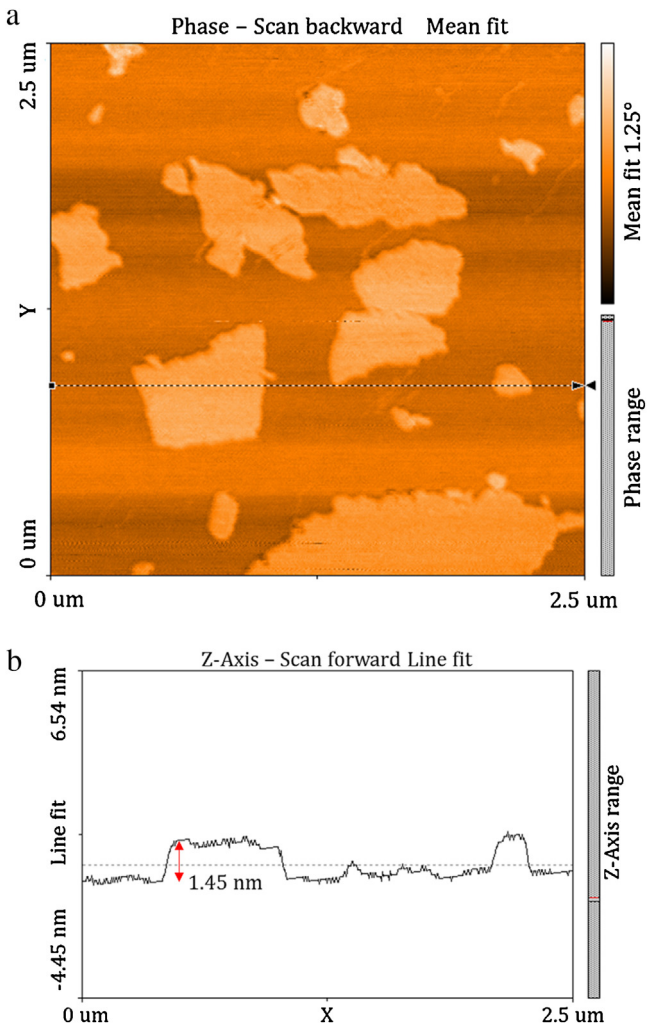

Fig. 1. AFM micrography of a dried GO suspension showing GO platelets (a). A representative cross-section shows the thickness of such platelets (b).

Table 1
GO content of the samples used in this study.

Code	BC dry weight (mg)	GO volume (mL)	GO content (%)
BC	14	–	0
BC/GO 10	14	0.75	9.7
BC/GO 20	14	2.00	22.2
BC/GO 30	14	3.00	30.0

2. Materials and methods

2.1. Bacterial cellulose production

All chemicals were analytical grade and used without purification. *Gluconacetobacter xylinus* was obtained from the Spanish type culture collection (CECT 473) and used to produce bacterial cellulose (BC) gels. The bacterium was cultured in broth media composed of 2% D-glucose, 0.5% yeast extract, 0.5% peptone, 0.27% $NaHPO_4$ and 0.115% citric acid. The cells were initially cultivated in a test tube until reaching a density of 3–5 × 10^8 cells/ml, which was determined by counting in a Neubauer chamber. At this point an inoculum was harvested, transferred to Erlenmeyer flasks containing 100 ml of the medium. The flasks were incubated statically for 14 days. The resulting BC gels were disks of approximately 40 mm in radius and 2 mm in thickness. At this point 20 ml of a 0.5 M NaOH solution was introduced in order to eliminate the cells and components of the culture liquid. The pH was then lowered to 7.0 by repeated washing with distilled water. The purified BC gels were stored in distilled water at 4 °C to prevent drying

2.2. Synthesis of BC/RGO

Graphene oxide dispersion (0.2 wt%) was purchased from Cheeptubes (USA). Dimensions of GO were 300–800 nm in width (Fig. 1a) and 0.7–1.5 nm in thickness (Fig. 1b). The dry weight of a pure BC film (~14 mg) was used as reference in order to calculate the volume of the GO dispersion needed to prepare the BC/GO films with a GO content of 10, 20 and 30% (Table 1).

Fig. 2 shows the processing route used to produce the BC nanocomposite films. A purified BC gel was carefully placed on a nitrocellulose membrane. The BC sample together with the nitrocellulose membrane was put on the Büchner funnel of a vacuum filtration kit (Fig. 2a). Then, the GO dispersion was poured over the BC gel and the vacuum pump was turned on. Vacuum filtration was

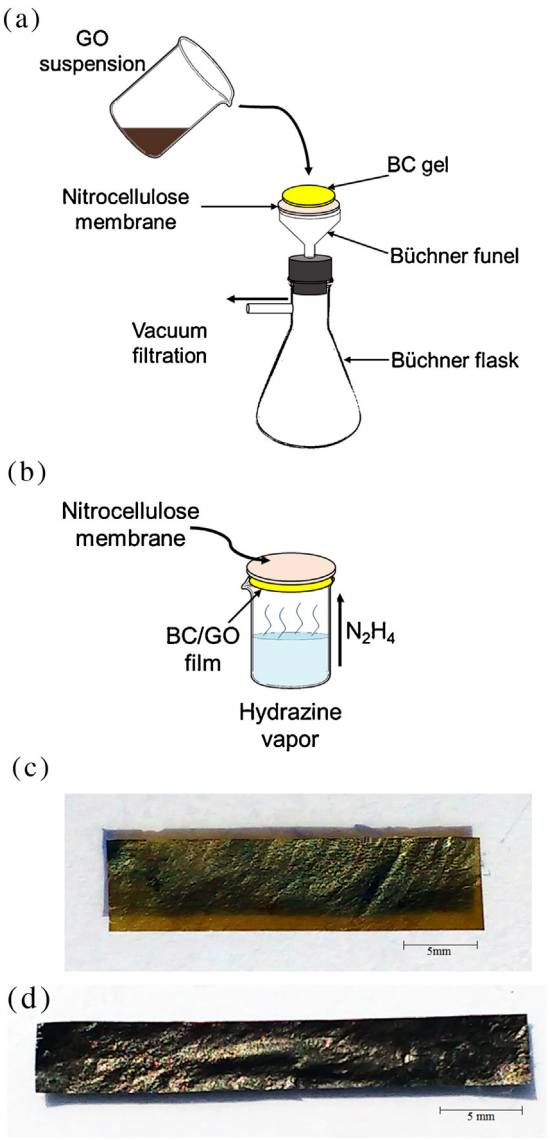

Fig. 2. Schematic illustration of the BC nanocomposite film preparation method (a) and the hydrazine treatment (b). The BC gel and GO dispersion are dried by vacuum filtration. The resulting dried BC/GO film is brown (c) and is and exposed to hydrazine vapors (3% v/v). The reduced films (BC/RGO) are black (d).

carried on for 30 min in order to extract water from the BC gel and to incorporate GO platelets into the BC network. The resulting BC/GO film was removed from the filtration set-up and oven-dried at 80 °C for 15 min. In order to in-situ reduce the incorporated GO, the dried BC/GO films were place on the top of a boiling hydrazine solution (3% v/v) for 5 and 15 min (Fig. 2b). Finally, the BC/RGO films were washed with distilled water three times and air-dried for 1 h. The thickness of the BC nanocomposites, measured with an Elcometer thickness gauge was around 5 μm.

2.3. Characterization techniques

Atomic force microscopy (AFM) was used to assess the dimensions of the GO platelets used in this study. A Nanosurf Easyscan 2 Atomic Force Microscope (AFM) in the dynamic mode was used. A cantilever with a nominal spring constant of 42 Nm-1, resonance frequency of 179 kHz and a tip radius lower than 10 nm was used.

Scanning electron micrography (SEM) was used to assess the morphology of the samples. SEM tests were carried out using a FEI Quanta 600 at 30 kV. Specimens were gold-sputter coating using a Polaron SC7640 Sputter Coater kit.

X-ray diffraction spectra were recorded using a Brucker D8 diffractometer with a copper laser and a Vantec-1 detector. Ni-filtered CuKα radiation (wavelength of 0.1542 nm) was produced at 40 kV and 40 mA. Scattered radiation was detected in the angular range of 0–70° (2θ) at a rate of 5°/min. The data were analyzed using specialized software (ANALYZE and DRXWin).

Tensile tests were performed in a tensile testing machine (Mark-10). Rectangular strips (4 mm x 5 μm) of dried samples were cut from the films and tested (across 5 samples per composition) with a load cell of 10 N. A crosshead speed of 10 mm/min was used. Tensile strength and Young's modulus values were recorded.

Thermogravimetry (TGA) experiments were carried in a Perkin Elmer Pyris TGA 4000. Scan rates of 10 °C/min in the temperature range 20–800 °C were used. The specimens were tested under a nitrogen atmosphere. BC, BC/GO and BC/RGO films were cut into small pieces and placed into ceramic pans. For pure GO tests, the GO dispersion was air-dried on a Petry dish in order to remove water. A mass of 10 mg was used in each TGA test.

DSC experiments were carried out in a Perkin Elmer DSC 4000 calorimeter. Aluminium pans were used. About 10 mg of the nanocomposite films were cut into small pieces and put inside the pans. Temperature scans from 0 to 450 °C were performed at 5 °C/min. All measurements were carried out under a nitrogen atmosphere (20 ml/min). Peak temperatures were recordered with the aid of Pyris® Thermal Analysis Software.

A Renishaw InVia Reflex Raman system coupled to an optical microscope was used to record spectra from the samples. A 512 nm IR-diode laser was focused on the sample with a x100 microscope objective. The Raman spectra from 600 to 3000 cm^{-1} were recorded using an exposure time of 10 s and three accumulations.

Attenuated total reflection Fourier transformed infrared spectroscopy tests were performed in a PERKIN ELMER SpectrumOne spectrophotometer equipped with a universal ATR sampling accessory, averaging 8 scans at a resolution of 4 cm^{-1} in the range from 4000 to 650 cm^{-1}. The data were analyzed by means of the IR Expert software.

The electrical conductivity of the BC films prepared was measured using a four-probe arrangement with a Fluke 175 multimeter and a 532C Metronix voltage source. The thickness of membranes (t) was precisely measured for calculating the electrical conductivity (σ) following Eq. (1):

$$\sigma = \frac{1}{\left(\frac{\pi}{\ln 2}\right)\left(\frac{V}{I}\right)t} \quad (1)$$

Where V and I stand for the voltage and current measured, respectively. For each measurement, three samples were tested three times at different positions along the surface, and then the average was reported.

3. Results and discussion

The processing route reported here is a simple method to incorporate graphene oxide (GO) platelets into BC gels to produce conductive BC based films. The morphology of samples is shown in Fig. 3. The typical coherent network made from the bacterial cellulose fibers can be observed in both, pure BC and reinforced samples (Fig. 3a–c). Agglomerations associated with the presence of GO platelets (Zhu et al., 2015) are observed in the cross-section of the BC/RGO sample (Fig. 3d). This shows that GO was successfully incorporated into the BC network.

Thermogravimetric tests were performed to confirm the incorporation of GO. Fig. 4a shows representative TGA thermograms of pure BC, GO and BC/GO films. Pure BC shows a weight loss that starts

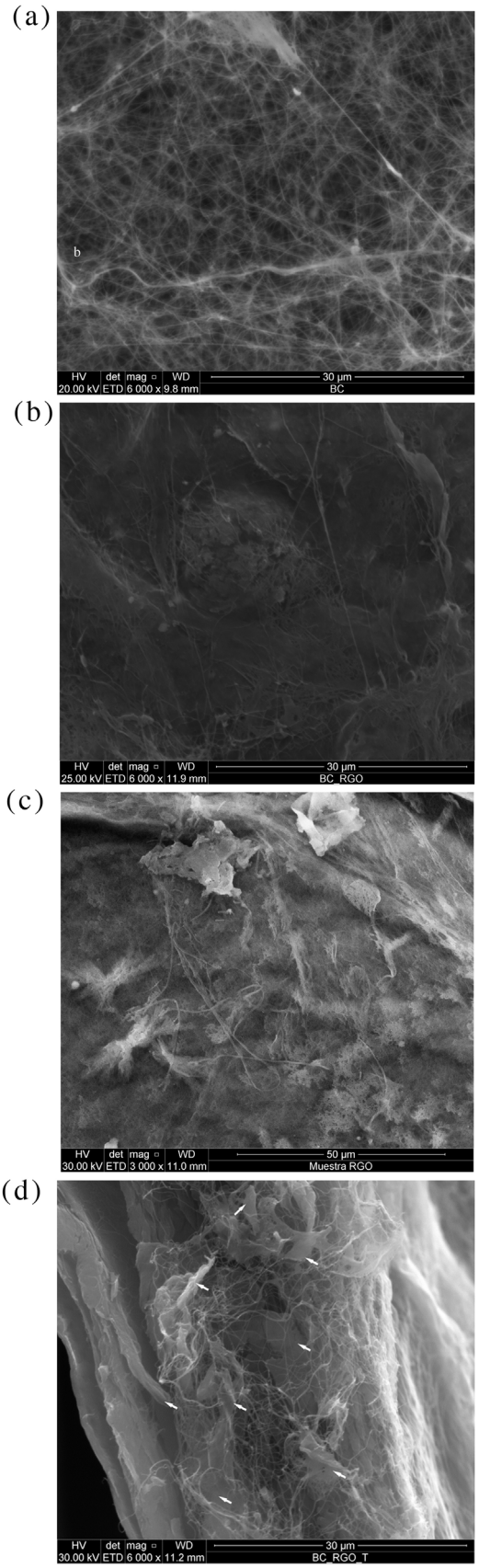

Fig. 3. SEM images of a representative pure BC film (a). The typical cellulose fibers are depicted. The upper (b) and lower surface (c) of a representative sample of a BC/RGO film is shown. A cross-sectional view of the BC/RGO sample is shown in (d). White arrows show agglomerations associated with the presence of RGO platelets.

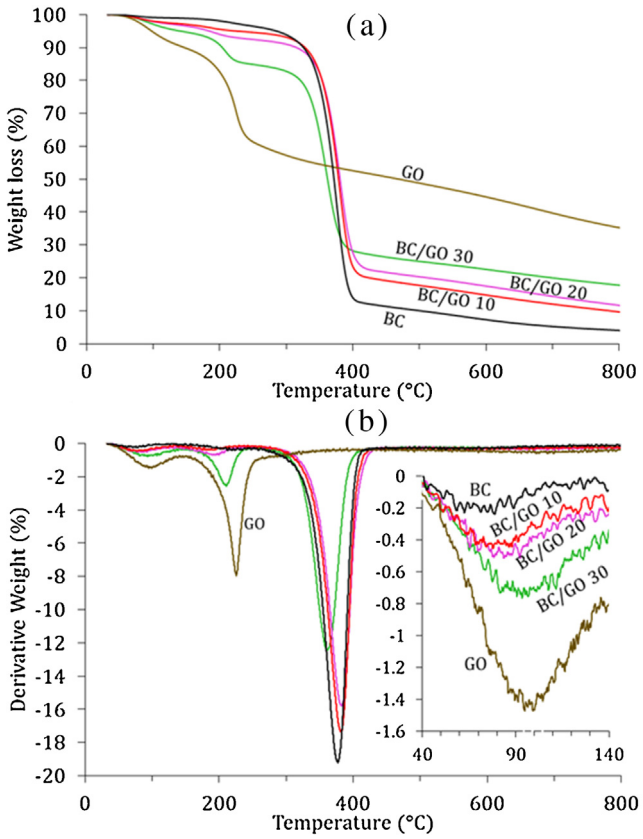

Fig. 4. Representative weight loss curves (a) and derivative of weight loss (b) of pure BC, GO and BC/GO films. Inset on (b) shows a detailed view of the peaks that take place at ~100 °C.

at ~320 °C. GO is thermally unstable and starts losing mass upon heating at 100 °C. A major mass loss associated with the pyrolysis of the labile oxygen-containing functional groups (Lerf, He, Forster, & Klinowski, 1998; Stankovich et al., 2007; Wang, Yang, Li, & Li, 2005) takes place at ~200 °C. The derivative TGA curves (Fig. 4b) show the presence of GO and BC peaks in the BC/GO curves.

The hydrazine treatment performed was aimed at in-situ reducing the incorporated GO. The effect of such treatment was first revealed by the change of color of the films. Before the hydrazine treatment, BC/GO films were brown. After the hydrazine treatment the color of the films changed to black, which is the color of RGO platelets (Fig. 2c and d). The hydrazine treatment also changed the thermal properties of the samples. Fig. 5 shows representative DSC curves of the samples. The BC thermogram shows an exothermic peak at ~204 ◦C associated with the degradation of proteinaceous matter and other debris, present in the native bacterial cellulose (George et al., 2005). BC/GO samples also show an exothermic peak at ~189 °C (Fig. 5a). This exothermic peak has been attributed to the reduction of GO (Qiu et al., 2014; Park et al., 2011) and was not found in the thermograms of the samples after the hydrazine treatment (Fig. 5b). The enthalpy of these exothermic peaks, calculated as the area below the peaks, was found to be dependent on the GO content of the sample. The enthalpy calculated was 138.46 J/g, 203.28 J/g and 233.8 J/g for the films with a GO content of 10%, 20% and 30%, respectively.

Tensile tests were carried out to assess the mechanical properties of the samples. Table 2 shows the elastic modulus and maximum strength of pure BC, BC/GO and BC/RGO films. It was found that the average value of the elastic modulus of pure BC films and films with a GO content of 10% and 20% is similar. A slightly improvement is achieved when the GO content is 30%. The

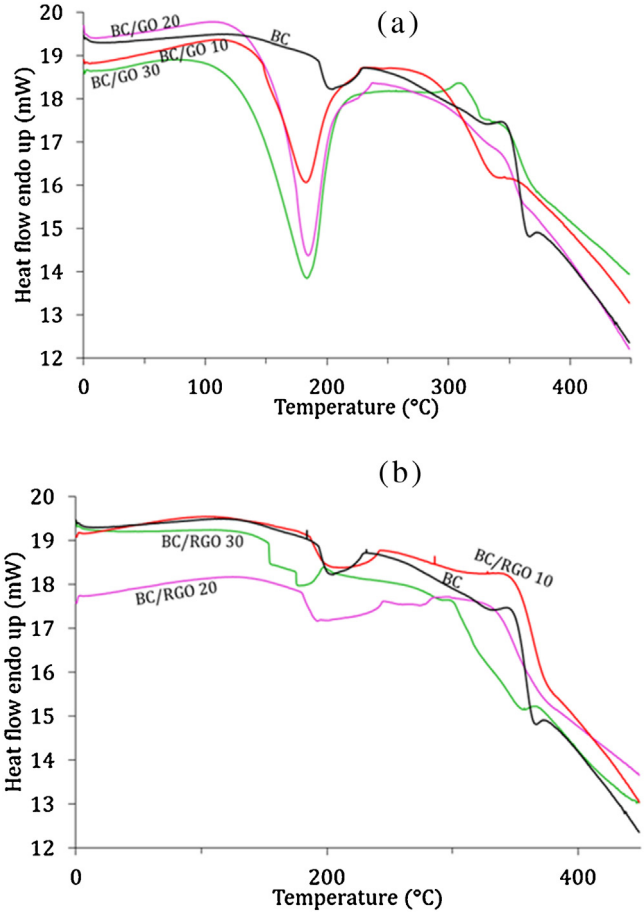

Fig. 5. DSC thermograms of BC nanocomposite films before (a) and after (b) hydrazine treatment.

Table 2
Maximum tensile strength and elastic modulus of BC, BC/GO and BC/RGO samples.

Code	Elastic modulus (GPa)	Maximum tensile strength (MPa)
BC	9.8 ± 1.7	151.81 ± 14
BC/GO 10	11.4 ± 0.4	140.3 ± 11.5
BC/GO 20	10.7 ± 2.2	77.7 ± 6.4
BC/GO 30	14.4 ± 1.7	184.85 ± 7.9
BC/RGO 10	11.3 ± 1.4	85.0 ± 11.4
BC/RGO 20	11.0 ± 0.4	70.92 ± 15.6
BC/RGO 30	13.2 ± 2.1	121.7 ± 19.0

fact that BC/GO and BC/RGO samples have similar elastic modulus shows that the hydrazine treatment has no effect on the mechanical properties of the samples. No correlation between the value of the maximum tensile strength and the GO content was found.

XRD tests were carried out in order to reveal changes on BC structure. Typical BC XRD patterns show peaks that correspond to the crystal planes of type I cellulose ($1\bar{1}0$), (110) and (200) (VanderHart & Atalla, 1984). The diffractograms of the samples prepared here show the same characteristic peaks at 14.8°, 17°, and 22.8° (Fig. 6). An additional peak at 34.5° (004) was observed for the BC/GO samples that were not exposed to hydrazine, but absent from those that had undergone exposure. The appearance of this peak at 34.5° may indicate a recover of crystallinity after hydrazine treatment. Following hydrazine treatment, molecular strains may relax due to the resulting generation of functional groups and chemical-physical bonds.

FTIR tests also showed changes with regard to pure BC films (Fig. 7). The spectrum of pure BC shows characteristic peaks

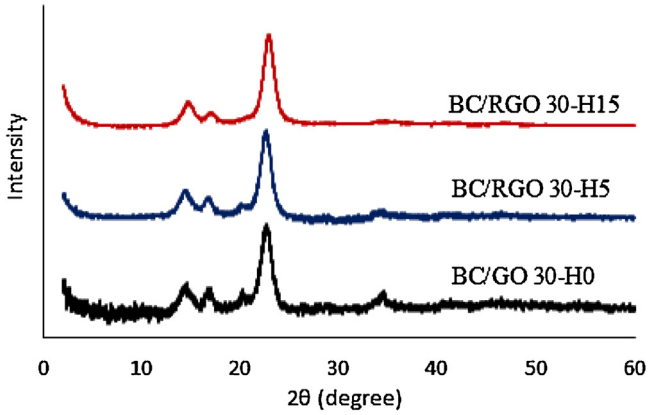

Fig. 6. Diffractograms of representative 30% BC/RGO films with varying durations of exposure to hydrazine vapor.

between 985 and 1106 cm^{-1} corresponding to the C—O bond stretching mainly attributed to primary alcohols. Previous studies on BC-based films carried out in this laboratory showed the same peaks (Grande, Torres, Gomez, & Carmen Bañó, 2009). The band at 1160 cm^{-1} is associated to the C—O—C asymmetric stretching and the peaks at 1315 and 1426 cm−1 are attributed to CH_2 wagging symmetric bending and CH_2 symmetric bending, respectively (Kačuráková, Smith, Gidley, & Wilson, 2002). The spectra of the BC/RGO composites are mainly dominated by the cellulose content. However, the hydrazine treatment seems to change the IR absorption of BC-based films. The intensity of the peak at 984 cm^{-1} (C—O bond stretching) that appears in pure BC weakens until it completely disappears from the spectrum of the samples with a hydrazine treatment of 15 min.

The presence of graphene in the films prepared here was confirmed with the Raman spectra. The Raman spectrum of carbon-based materials may present three characteristic peaks: the G band, the D band and the 2D (or G') band. The G band is common to all the graphitic samples, is due to in-plane vibration of sp^2 carbon atoms, and is a doubly degenerate phonon mode (E_{2g} symmetry) at the Brillouin zone center (Pimenta et al., 2007; Tuinstra & Koenig, 1970). The D band is due to a one-phonon second order Raman scattering process associated with the finite size of crystals and carbonaceous defects (Ferrari, 2007). The 2D band is indicative of a two-phonon second order Raman scattering process associated to zone-boundary phonons (DiLeo, Landi, & Raffaelle, 2007).

Fig. 8 shows the Raman spectrum of representative BC/RGO films after the hydrazine treatment at different times. The typical G-, D- and 2D band can be observed. The BC/RGO samples show a broad 2D band. This 2D-band has been widely used to identify the number of graphene layers (Ferrari et al., 2006; Ferrari, 2007; Graf et al., 2007; Gupta, Chen, Joshi, Tadigadapa, & Eklund, 2006). A sharp symmetric peak corresponds to single layer graphene whereas broad peaks are associated with multi-layer graphene.

Raman spectroscopy is also used to study defects in graphitic materials such as vacancy-type and sp^3-defects (Eckmann et al., 2012; Koppens, Chang, & de Abajo, 2011; Lucchese et al., 2010; Martins Ferreira et al., 2010). The D-band is activated by a single-phonon inter-valley scattering process where the defect provides the missing momentum in order to satisfy momentum conservation in the Raman scattering process (Basko, 2008; Saito et al., 2001; Thomsen & Reich, 2000; Venezuela, Lazzeri, & Mauri, 2011). Thus, the intensity ratio of the D and G band (I_D/I_G) is commonly used to evaluate the quality of carbon materials (Kudin et al., 2008). A low I_D/I_G ratio corresponds to a low defect structure.

We have used the empirical Eq. (2) proposed by the Tuinstra-Koenig relation (Tuinstra & Koenig, 1970), which relates the I_D/I_G

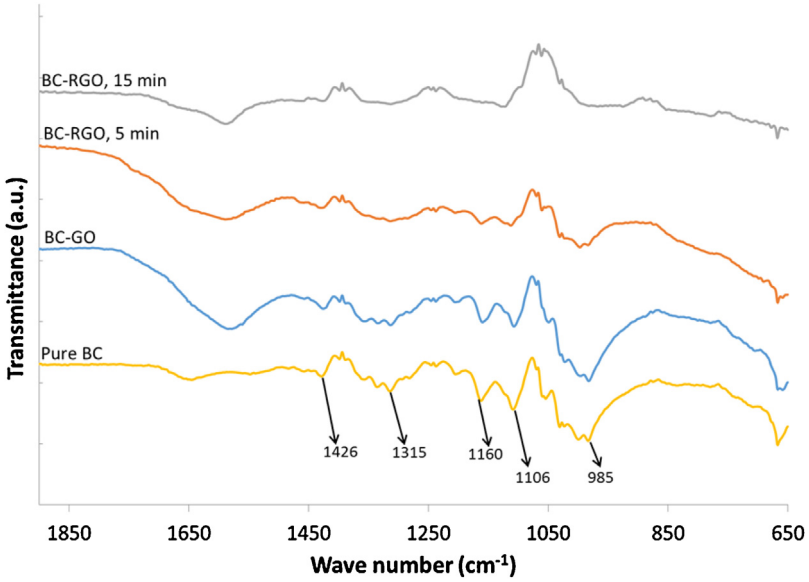

Fig. 7. FTIR spectra of 30% BC/RGO films with varying durations of exposure to hydrazine vapor. Arrows show the typical bands associated to cellulose.

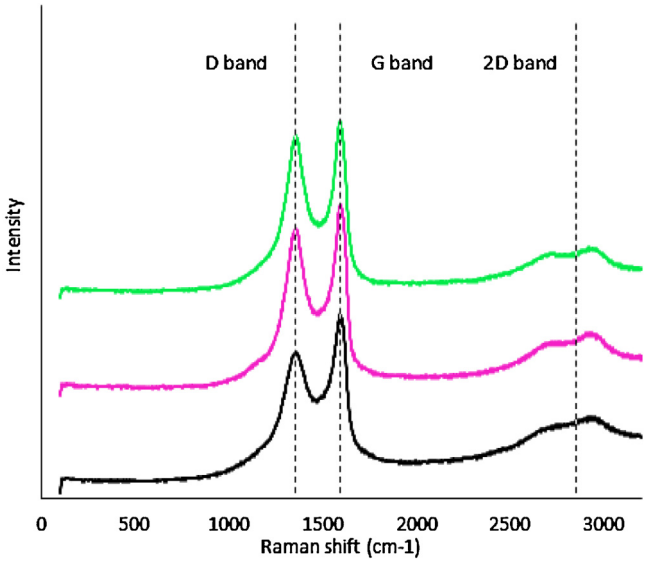

Fig. 8. Raman spectra of representative 30% BC/RGO compounds with varying durations of exposure to hydrazine vapor. The D, G and 2D bands associated to graphene are shown.

intensity ratio to the crystallite size (L_a) of graphitic samples as follows:

$$I_D/I_G = C(\lambda)/L_a \quad (2)$$

Where $C(\lambda)$ is an empirical constant that depends on the excitation wavelength. In this case $\lambda = 514$ nm and $C = 4.4$ nm. Our calculations show that the GO/RGO platelets used here are comprised of ordered graphitic regions with a size of ~4.8–4.6 nm.

Fig. 8 shows that the I_D/I_G ratio increases with the hydrazine treatment time from 0.79 (no hydrazine treatment) to 0.92 (15 min of hydrazine treatment). This suggests that the number of defects increases with increasing hydrazine treatment times. The processing technique reported here allows for incorporation of graphene oxide into the BC network. The hydrazine treatment reduces the previously incorporated graphene oxide and forms the BC/RGO nanocomposites.

We have used graphene oxide as a starting material for the preparation of BC/RGO films. As opposed to micromechanical cleaved pristine graphene, the basal plane of graphene oxide platelets are decorated with epoxy and hydroxyl groups and the edge carbon atoms bear carbonyl and carboxyl groups (He, Klinowski, Forster, & Lerf, 1998; Lerf et al., 1998; Schniepp et al., 2006). During the oxidation process used to manufacture graphene oxide the aromaticity of the graphene sheets is lost as epoxy and hydroxyl groups are formed. Schniepp et al. (Schniepp et al., 2006) reports that the interlayer spacing (d-spacing) of graphene sheets is 0.34 nm whereas the spacing of graphene oxide sheets is 0.7 nm. Epoxy and hydroxyl functional groups are randomly distributed on the starting graphene oxide sheets. The hydrazine treatment performed here removes some of the epoxy and hydroxyl groups (Fig. 9).

Park et al. (2012) have reported the use of hydrazine to reduce graphene oxide. They carried out NMR tests and found that hydroxyl groups on the basal plane of graphene were mostly removed and 1,2-epoxide groups on the basal planes were completely removed by the hydrazine treatment. They proposed that the reduction of graphene oxide restores the sp^2 networks on the basal planes while reducing the concentration of hydroxyl and 1,2-epoxide groups. Hydrazine-based treatments have been shown to effectively remove a large fraction of the oxygen-based functional groups and increase the content of non-oxygenated carbon. The carbon/oxygen ratio of graphene oxide has been shown to increase from ~1 to ~10 after hydrazine reduction (Liang et al., 2009; Si & Samulski, 2008; Wang et al., 2008).

The hydrazine treatment is necessary to produce conductive BC-based films. Graphene oxide (without hydrazine treatment) is highly oxidized with disrupted π conjugation and therefore exhibits low electrical conductivity (Acik et al., 2010; Li, Muller, Gilje, Kaner, & Wallace, 2008; Wassei & Kaner, 2010). Pure BC and untreated samples behaved close-to insulating materials with conductivity values too low to be measured by the 4-probe setup used here.

Pure BC is not a conductive material. As expected, the conductivity of samples treated with hydrazine was dependent on the RGO content. Fig. 10 shows that the conductivity of the samples increases sharply at a RGO concentration of 30%. This suggests that a percolation mechanism may be behind this behavior.

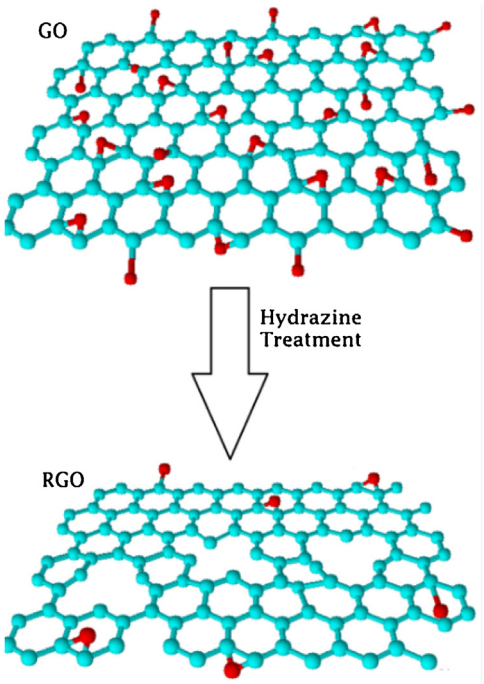

Fig. 9. Schematic representation of graphene oxide (GO). Different studies suggest that the oxygen-containing groups (red beads) are clustered into rows and islands. This scheme shows graphitic regions intermixed with islands of oxygen-functionalized atoms. The hydrazine treatment removes some of the oxygen-containing forming a reduced graphene oxide (RGO). The resulting RGO presents defects as hydroxyl and epoxy groups are removed. (For interpretation of the references to color in this figure legend, the reader is referred to the web version of this article.)

For the samples with 10% and 20% of RGO content, the increase of the hydrazine treatment time (from 5 min to 15 min) had a limited effect on their conductivity. However, for the samples with a RGO content of 30%, the conductivity value of the samples treated for 15 min reached 12 S/m and it was more than 3 times the conductivity of the samples treated for only 5 min. This conductivity is higher than the one reported by Feng et al. (Feng et al., 2012) (5×10^{-3} S/m) for BC based composites reinforced with 10% of RGO. Liu et al. (Liu et al., 2015) prepared BC films reinforced with 15.6% of RGO with a conductivity of 171 S/m. However, the processing technique used by Liu et al. (Liu et al., 2015) required the disintegration of the native BC structure and, thus, a decrease on the mechanical properties. The elastic modulus of the BC/RGO films prepared by Liu et al. (Liu et al., 2015) was 0.077 GPa. In contrast, the elastic modulus of the BC/RGO prepared in this study ranged 11.0–13.2 GPa.

The hydrazine treatment used here is very efficient for increasing the conductivity of the BC/RGO nanocomposites. It has been suggested that the reestablishment of carbon rings and the π-π bonding in graphene via hydrazine is quite efficient (Lin & Grossman, 2015; Park et al., 2012). Here we implemented a simple method to reduce BC/GO using a low concentration of hydrazine (3%) and a brief period of exposure. This treatment increases the content of non-oxygenated carbon and causes a significant boost in electrical performance of the BC/RGO films.

4. Conclusions

We have reported a novel processing technique to obtain BC/GO films with enhanced conductivity. We have shown that the graphene oxide platelets incorporated into the BC network can be in-situ reduced by means of a hydrazine treatment to form reduced graphene oxide. This treatment removes the hydroxyl and epoxy groups present on the reduced graphene, increases the content of nonoxygenated carbon and increases the conductivity of the BC-based films more than 3 times. The BC/RGO films prepared through this fast in-situ technique might found several potential applications as substrates for engineered scaffolds with electrical stimulation, biosensors, electrical biointerfaces for transmitting or collecting physiological signals and materials for energy devices. Further studies are needed in order to determine if this process could be used with other types of cellulosic materials such as plant cellulose.

Acknowledgements

The authors would like to thank the Peruvian Council of Science and Technology (Concytec-FONDECYT) and the Vice-Rectorate for Research of the Pontificia Universidad Catolica del Peru (VRI-PUCP) for financial support. RC would like to thank the Peruvian Coun-

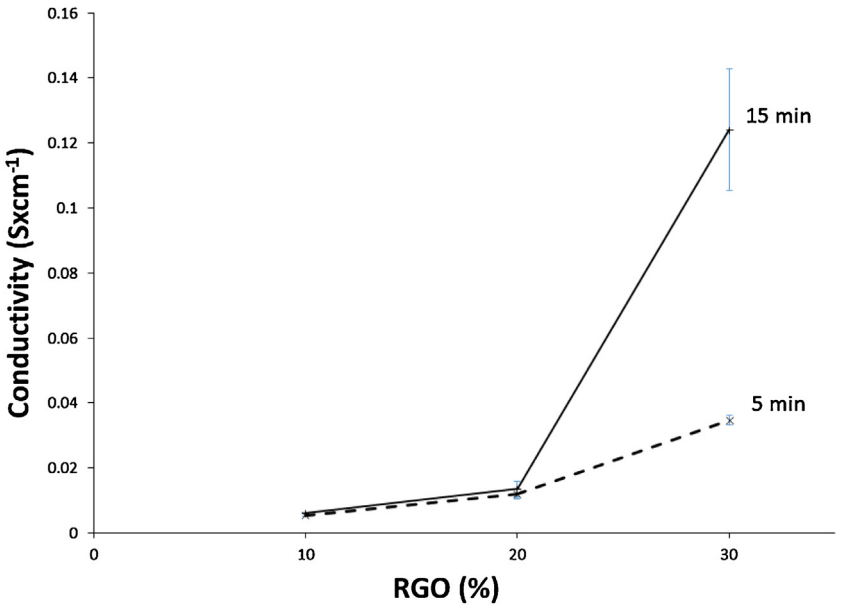

Fig. 10. Variation of conductivity with the RGO content before and after hydrazine treatment for 5 min and 10 min.

cil of Science and Technology (Concytec-FONDECYT) for financial support.

References

Acik, M., Lee, G., Mattevi, C., Chhowalla, M., Cho, K., & Chabal, Y. J. (2010). Unusual infrared-absorption mechanism in thermally reduced graphene oxide. *Nature Materials*, *9*(10), 840–845.

Basko, D. M. (2008). Theory of resonant multiphonon Raman scattering in graphene. *Physical Review B*, *78*(12), 125418. https://doi.org/10.1103/PhysRevB.78.125418

Bella, F., Mobarak, N. N., Jumaah, F. N., & Ahmad, A. (2015). From seaweeds to biopolymeric electrolytes for third generation solar cells: an intriguing approach. *Electrochimica Acta*, *151*, 306–311. https://doi.org/10.1016/j.electacta.2014.11.058

Buraidah, M. H., Teo, L. P., Majid, S. R., Yahya, R., Taha, R. M., & Arof, A. K. (2010). Characterizations of chitosan-based polymer electrolyte photovoltaic cells. *International Journal of Photoenergy*, *2010*, 1–7. https://doi.org/10.1155/2010/805836

Culebras, M., Grande, C. J., Torres, F. G., Troncoso, O. P., Gomez, C. M., & Bañó, M. C. (2015). Optimization of cell growth on bacterial cellulose by adsorption of collagen and poly-L-lysine. *International Journal of Polymeric Materials and Polymeric Biomaterials*, *64*(8), 411–415. https://doi.org/10.1080/00914037.2014.958829

DiLeo, R. A., Landi, B. J., & Raffaelle, R. P. (2007). Purity assessment of multiwalled carbon nanotubes by Raman spectroscopy. *Journal of Applied Physics*, *101*(6), 064307. https://doi.org/http://dx.doi.org/10.1063/1.2712152

Eckmann, A., Felten, A., Mishchenko, A., Britnell, L., Krupke, R., Novoselov, K. S., & Casiraghi, C. (2012). Probing the nature of defects in graphene by Raman spectroscopy. *Nano Letters*, *12*(8), 3925–3930. https://doi.org/10.1021/nl300901a

Feng, Y., Zhang, X., Shen, Y., Yoshino, K., & Feng, W. (2012). A mechanically strong, flexible and conductive film based on bacterial cellulose/graphene nanocomposite. *Carbohydrate Polymers*, *87*(1), 644–649. https://doi.org/10.1016/j.carbpol.2011.08.039

Ferrari, A. C., Meyer, J. C., Scardaci, V., Casiraghi, C., Lazzeri, M., Mauri, F., & Geim, A. K. (2006). Raman spectrum of graphene and graphene layers. *Physical Review Letters*, *97*(18), 187401. https://doi.org/10.1103/PhysRevLett.97.187401

Ferrari, A. C. (2007). Raman spectroscopy of graphene and graphite: Disorder, electron-phonon coupling, doping and nonadiabatic effects. *Solid State Communications*, *143*(1-2), 47–57. https://doi.org/http://dx.doi.org/10.1016/j.ssc.2007.03.052

Gan, L., Shang, S., Yuen, C. W. M., & Jiang, S. (2015). Graphene nanoribbon coated flexible and conductive cotton fabric. *Composites Science and Technology*, *117*, 208–214. https://doi.org/http://dx.doi.org/10.1016/j.compscitech.2015.06.019

Gelin, K., Bodin, A., Gatenholm, P., Mihranyan, A., Edwards, K., & Strømme, M. (2007). Characterization of water in bacterial cellulose using dielectric spectroscopy and electron microscopy. *Polymer*, *48*(26), 7623–7631. https://doi.org/http://dx.doi.org/10.1016/j.polymer.2007.10.039

Graf, D., Molitor, F., Ensslin, K., Stampfer, C., Jungen, A., Hierold, C., & Wirtz, L. (2007). Spatially resolved Raman spectroscopy of single- and few-layer graphene. *Nano Letters*, *7*(2), 238–242.

Grande, C. J., Torres, F. G., Gomez, C. M., & Carmen Bañó, M. (2009). Nanocomposites of bacterial cellulose/hydroxyapatite for biomedical applications. *Acta Biomaterialia*, *5*(5), 1605–1615. https://doi.org/10.1016/j.actbio.2009.01.022

Grande, C. J., Torres, F. G., Gomez, C. M., Troncoso, O. P., Canet-Ferrer, J., & Martínez-Pastor, J. (2009). Development of self-assembled bacterial cellulose-starch nanocomposites. *Materials Science and Engineering: C*, *29*(4), 1098–1104. https://doi.org/http://dx.doi.org/10.1016/j.msec.2008.09.024

Gupta, A., Chen, G., Joshi, P., Tadigadapa, S., & Eklund, P. C. (2006). Raman scattering from high-frequency phonons in supported n-graphene layer films. *Nano Letters*, *6*(12), 2667–2673. https://doi.org/10.1021/nl061420a

He, H., Klinowski, J., Forster, M., & Lerf, A. (1998). A new structural model for graphite oxide. *Chemical Physics Letters*, *287*(1–2), 53–56. https://doi.org/http://dx.doi.org/10.1016/S0009-2614(98)00144-4

Hu, W., Chen, S., Yang, Z., Liu, L., & Wang, H. (2011). Flexible electrically conductive nanocomposite membrane based on bacterial cellulose and polyaniline. *Journal of Physical Chemistry B*, *115*(26), 8453–8457. https://doi.org/10.1021/jp204422v

Iguchi, M., Yamanaka, S., & Budhiono, A. (2000). Bacterial cellulose—A masterpiece of nature's arts. *Journal of Materials Science*, *35*(2), 261–270. https://doi.org/10.1023/A:1004775229149

Kačuráková, M., Smith, A. C., Gidley, M. J., & Wilson, R. H. (2002). Molecular interactions in bacterial cellulose composites studied by 1D FT-IR and dynamic 2D FT-IR spectroscopy. *Carbohydrate Research*, *337*(12), 1145–1153. https://doi.org/http://dx.doi.org/10.1016/S0008-6215(02)00102-7

Koppens, F. H. L., Chang, D. E., & de Abajo, F. J. G. (2011). Graphene plasmonics: A platform for strong light—matter interactions. *Nano Letters*, *11*(8), 3370–3377.

Kudin, K. N., Ozbas, B., Schniepp, H. C., Prud'homme, R. K., Aksay, I. A., & Car, R. (2008). Raman spectra of graphite oxide and functionalized graphene sheets. *Nano Letters*, *8*(1), 36–41. https://doi.org/10.1021/nl071822y

Lay, M., González, I., Tarrés, J. A., Pellicer, N., Bun, K. N., & Vilaseca, F. (2017). High electrical and electrochemical properties in bacterial cellulose/polypyrrole membranes. *European Polymer Journal*, https://doi.org/http://dx.doi.org/10.1016/j.eurpolymj.2017.03.021

Lee, T.-W., Han, M., Lee, S.-E., & Jeong, Y. G. (2016). Electrically conductive and strong cellulose-based composite fibers reinforced with multiwalled carbon nanotube containing multiple hydrogen bonding moiety. *Composites Science and Technology*, *123*, 57–64. https://doi.org/http://dx.doi.org/10.1016/j.compscitech.2015.12.006

Lerf, A., He, H., Forster, M., & Klinowski, J. (1998). Structure of graphite oxide revisited. *The Journal of Physical Chemistry B*, *102*(23), 4477–4482. https://doi.org/10.1021/jp9731821

Li, D., Muller, M. B., Gilje, S., Kaner, R. B., & Wallace, G. G. (2008). Processable aqueous dispersions of graphene nanosheets. *Nat Nano*, *3*(2), 101–105.

Liang, J., Wang, Y., Huang, Y., Ma, Y., Liu, Z., Cai, J., & Chen, Y. (2009). Electromagnetic interference shielding of graphene/epoxy composites. *Carbon*, *47*(3), 922–925. https://doi.org/http://dx.doi.org/10.1016/j.carbon.2008.12.038

Lin, L.-C., & Grossman, J. C. (2015). Atomistic understandings of reduced graphene oxide as an ultrathin-film nanoporous membrane for separations. *Nature Communications*, *6*, 8335. https://doi.org/10.1038/ncomms9335

Liu, Y., Zhou, J., Zhu, E., Tang, J., Liu, X., & Tang, W. (2015). A facile synthesis of bacterial cellulose fibers covalently intercalated graphene oxide by one-step cross-linking for robust supercapacitors. *Journal of Materials Chemistry C*, *3*, 1011–1017. https://doi.org/10.1039/b000000x

Lucchese, M. M., Stavale, F., Ferreira, E. H. M., Vilani, C., Moutinho, M. V. O., Capaz, R. B., & Jorio, A. (2010). Quantifying ion-induced defects and Raman relaxation length in graphene. *Carbon*, *48*(5), 1592–1597. https://doi.org/http://dx.doi.org/10.1016/j.carbon.2009.12.057

Luo, H., Xiong, G., Yang, Z., Raman, S. R., Si, H., & Wan, Y. (2014). A novel three-dimensional graphene/bacterial cellulose nanocomposite prepared by in situ biosynthesis. *RSC Adv.*, *4*(28), 14369–14372. https://doi.org/10.1039/C4RA00318G

Martins Ferreira, E. H., Moutinho, M. V. O., Stavale, F., Lucchese, M. M., Capaz, R. B., Achete, C. A., & Jorio, A. (2010). Evolution of the Raman spectra from single-, few-, and many-layer graphene with increasing disorder. *Phys. Rev. B*, *82*(12), 125429. https://doi.org/10.1103/PhysRevB.82.125429

Mormino, R., & Bungay, H. (2003). Composites of bacterial cellulose and paper made with a rotating disk bioreactor. *Applied Microbiology and Biotechnology*, *62*(5), 503–506. https://doi.org/10.1007/s00253-003-1377-5

Nandgaonkar, A. G., Wang, Q., Fu, K., Krause, W. E., Wei, Q., Gorga, R., & Lucia, A. L. (2014). A one-pot biosynthesis of reduced graphene oxide (RGO)/bacterial cellulose (BC) nanocomposites. *Green Chemistry*, *16*(6), 3195–3201. https://doi.org/10.1039/C4GC00264D

Park, S., Hu, Y., Hwang, J. O., Lee, E.-S., Casabianca, L. B., Cai, W., & Ruoff, R. S. (2012). Chemical structures of hydrazine-treated graphene oxide and generation of aromatic nitrogen doping. *Nature Communications*, *3*, 638. https://doi.org/10.1038/ncomms1643

Pimenta, M. A., Dresselhaus, G., Dresselhaus, M. S., Cancado, L. G., Jorio, A., & Saito, R. (2007). Studying disorder in graphite-based systems by Raman spectroscopy. *Phys. Chem. Chem. Phys.*, *9*(11), 1276–1290. https://doi.org/10.1039/B613962K

Rudhziah, S., Ahmad, A., Ahmad, I., & Mohamed, N. S. (2015). Biopolymer electrolytes based on blend of kappa-carrageenan and cellulose derivatives for potential application in dye sensitized solar cell. *Electrochimica Acta*, *175*, 162–168. https://doi.org/10.1016/j.electacta.2015.02.153

Saito, R., Jorio, A., Souza Filho, A. G., Dresselhaus, G., Dresselhaus, M. S., & Pimenta, M. A. (2001). Probing phonon dispersion relations of graphite by double resonance Raman scattering. *Physical Review Letters*, *88*(2), 27401. https://doi.org/10.1103/PhysRevLett.88.027401

Schniepp, H. C., Li, J.-L., McAllister, M. J., Sai, H., Herrera-Alonso, M., & Adamson, D. H. (2006). Functionalized single graphene sheets derived from splitting graphite oxide. *The Journal of Physical Chemistry B*, *110*(17), 8535–8539.

Shi, Z., Li, Y., Chen, X., Han, H., & Yang, G. (2014). Double network bacterial cellulose hydrogel to build a biology-device interface. *Nanoscale*, *6*(2), 970–977. https://doi.org/10.1039/c3nr05214a

Si, Y., & Samulski, E. T. (2008). Synthesis of water soluble graphene. *Nano Letters*, *8*(6), 1679–1682. https://doi.org/10.1021/nl080604h

Si, H., Luo, H., Xiong, G., Yang, Z., Raman, S. R., Guo, R., & Wan, Y. (2014). One-step in situ biosynthesis of graphene oxide-bacterial cellulose nanocomposite hydrogels. *Macromolecular Rapid Communications*, *35*(19), 1706–1711. https://doi.org/10.1002/marc.201400239

Stankovich, S., Dikin, D. A., Piner, R. D., Kohlhaas, K. A., Kleinhammes, A., Jia, Y., & Ruoff, R. S. (2007). Synthesis of graphene-based nanosheets via chemical reduction of exfoliated graphite oxide. *Carbon*, *45*(7), 1558–1565. https://doi.org/http://dx.doi.org/10.1016/j.carbon.2007.02.034

Svensson, A., Nicklasson, E., Harrah, T., Panilaitis, B., Kaplan, D. L., Brittberg, M., & Gatenholm, P. (2005). Bacterial cellulose as a potential scaffold for tissue engineering of cartilage. *Biomaterials*, *26*(4), 419–431. https://doi.org/http://dx.doi.org/10.1016/j.biomaterials.2004.02.049

Thomsen, C., & Reich, S. (2000). Double resonant Raman scattering in graphite. *Physical Review Letters*, *85*(24), 5214–5217. https://doi.org/10.1103/PhysRevLett.85.5214

Tian, M., Qu, L., Zhang, X., Zhang, K., Zhu, S., Guo, X., & Sun, Y. (2014). Enhanced mechanical and thermal properties of regenerated cellulose/graphene composite fibers. *Carbohydrate Polymers*, *111*, 456–462. https://doi.org/http://dx.doi.org/10.1016/j.carbpol.2014.05.016

Tuinstra, F., & Koenig, J. L. (1970). Raman spectrum of graphite. *The Journal of Chemical Physics*, *53*(3), 1126.

VanderHart, D. L., & Atalla, R. H. (1984). Studies of microstructure in native celluloses using solid-state carbon-13 NMR. *Macromolecules*, *17*(8), 1465–1472. https://doi.org/10.1021/ma00138a009

Venezuela, P., Lazzeri, M., & Mauri, F. (2011). Theory of double-resonant Raman spectra in graphene: Intensity and line shape of defect-induced and two-phonon bands. *Physical Review B*, *84*(3), 35433. https://doi.org/10.1103/PhysRevB.84.035433

Wang, G., Yang, Z., Li, X., & Li, C. (2005). Synthesis of poly(aniline-co-o-anisidine)-intercalated graphite oxide composite by delamination/reassembling method. *Carbon*, *43*(12), 2564–2570. https://doi.org/http://dx.doi.org/10.1016/j.carbon.2005.05.008

Wang, G., Yang, J., Park, J., Gou, X., Wang, B., Liu, H., & Yao, J. (2008). Facile synthesis and characterization of graphene nanosheets. *The Journal of Physical Chemistry C*, *112*(22), 8192–8195. https://doi.org/10.1021/jp710931h

Wassei, J. K., & Kaner, R. B. (2010). Graphene, a promising transparent conductor. *Materials Today*, *13*(3), 52–59. https://doi.org/http://dx.doi.org/10.1016/S1369-7021(10)70034-1

Yamanaka, S., Watanabe, K., Kitamura, N., Iguchi, M., Mitsuhashi, S., Nishi, Y., & Uryu, M. (1989). The structure and mechanical properties of sheets prepared from bacterial cellulose. *Journal of Materials Science*, *24*(9), 3141–3145. https://doi.org/10.1007/BF01139032

Yano, H. (2005). Optically transparent composites reinforced with networks of bacterial nanofibers. *Sustainable Humanosphere*, *1*, 11. https://doi.org/10.1002/adma.200400597

Zhang, X., Liu, X., Zheng, W., & Zhu, J. (2012). Regenerated cellulose/graphene nanocomposite films prepared in DMAC/LiCl solution. *Carbohydrate Polymers*, *88*(1), 26–30. https://doi.org/http://dx.doi.org/10.1016/j.carbpol.2011.11.054

Zhu, W., Li, W., He, Y., & Duan, T. (2015). In-situ biopreparation of biocompatible bacterial cellulose/graphene oxide composites pellets. *Applied Surface Science*, *338*, 22–26. https://doi.org/10.1016/j.apsusc.2015.02.030

Zimmermann, T., Bordeanu, N., & Strub, E. (2010). Properties of nanofibrillated cellulose from different raw materials and its reinforcement potential. *Carbohydrate Polymers*, *79*(4), 1086–1093. https://doi.org/http://dx.doi.org/10.1016/j.carbpol.2009.10.045